# Numerical Simulations of Freely Oscillating Drops

**Jorge Troconis, Armando Blanco, Dominique Legendre, Leonardo Trujillo and Leonardo Di G. Sigalotti**

**Abstract** The non-linear oscillations of a viscous drop is a fundamental problem in diverse areas of science and technology. In this paper, we analyze the large-amplitude oscillations of an initially elongated liquid drop in two-dimensions by solving the free boundary problem comprised of the Navier-Stokes equations, using two different numerical codes. The drop models all start from the same deformation in vacuum with zero gravity and varied Reynolds numbers (Re). We find that non-isothermal drops undergo stronger damping than isothermal ones due to the additional dissipative effects of heat conduction. Regardless of the drop parameters and physical mechanisms of dissipation, the transition from periodic to aperiodic decay is seen to occur for Re $\leq$ 1.5 in good agreement with linear theory and previous numerical simulations.

J. Troconis (✉) · L. Di G. Sigalotti · L. Trujillo
Centro de Física, Instituto Venezolano de Investigaciones Científicas, IVIC, Apartado Postal 20632, Caracas 1020-A, Venezuela
e-mail: jorge.troconi@gmail.com

A. Blanco
Departamento de Mecánica,Universidad Simón Bolívar, USB, Caracas 1080, Venezuela
e-mail: ajblanco@usb.ve

D. Legendre
Institut de Mécanique des Fluides de Toulouse, IMFT,Université de Toulouse, CNRS-INPT-UPS, 2 Allée du Professeur Camille Soula, 31400 Toulouse, France
e-mail: dominique.legendre@imft.fr

L. Trujillo
The Abdus Salam International Centre for Theoretical Physics, ICTP, Strada Costiera 11, 34014 Trieste, Italy
e-mail: leonardo.trujillo@gmail.com

L. Di G. Sigalotti et al. (eds.), *Computational and Experimental Fluid Mechanics with Applications to Physics, Engineering and the Environment*, Environmental Science and Engineering,
DOI:10.1007/978-3-319-00191-3_20, 

## 1 Introduction

The free oscillations of liquid drops have been studied extensively over more than a century, both for the sake of basic scientific understanding as well as for their dumbfounding applications in the chemical, pharmaceutical, and food industry. The problem has applications in polymer processing, dispersion technologies, gene chip arraying, inkjet printing, catalyst production, containerless processing technology in space, and metereology among many others. In the absence of gravity, the infinitesimal-amplitude oscillations of a drop were first shown to be correlated to its surface tension, density, and size (Rayleigh 1879). Here by oscillations we refer to periodic changes of the drop surface shape from spherical to ellipsoidal and back. A few other analyses for viscous drops have been reported in the literature (Reid 1960; Miller and Scriven 1968; Prosperetti 1980). It was shown that the initial motion of a viscous drop is just that executed by a damped harmonic oscillator of natural frequency $\omega_n' = (\omega_n^2 - b_n^2)^{1/2}$, for which the amplitude decays exponentially with time, where $\omega_n$ is the Rayleigh frequency (Rayleigh 1879) and $b_n$ is a damping parameter depending on the drop density, size, and dynamic viscosity. Moreover, a transition from periodic to aperiodic decay of the oscillations was found to occur between Re $\approx$ 1.3 and 1.768 (Prosperetti 1980), where Re is the Reynolds number.

For inviscid drops undergoing slightly non-linear oscillations, the oscillation frequency was shown to decrease with increasing initial amplitude (Tsamopoulos and Brown 1983). On the other hand, numerical simulations of large-amplitude oscillations of slightly viscous drops have revealed that even a small viscosity may have a relatively large effect on resonant-mode coupling (Lundgren and Mansour 1988). Simulations addressed to study the effects of finite viscosity on large-amplitude, oscillating drops were also considered by a number of authors (Basaran 1992; Becker et al. 1994; Mashayek and Ashgriz 1998; Meradji et al. 2001; Moran et al. 2003; López and Sigalotti 2006). These calculations have revealed that frequency modulation and mode coupling are dominant, even for small initial deformations (Becker et al. 1994), whereas internal circulation may have significant effects on the frequency and damping rate during the first few periods of oscillation (Mashayek and Ashgriz 1998). In the absence of internal circulation, the damping rate is essentially governed by the combined action of viscous and surface tension forces (López and Sigalotti 2006).

Experimental observations of acoustically levitated drops have confirmed qualitatively the behaviour predicted by the linear and non-linear theory (Trinh and Wang 1982). For instance, mode coupling and asymmetries in the oscillation amplitude of high-order modes have been observed in drops with initial $n = 2$ deformations larger than about 10 % of their spherical radius (Becker et al. 1991). Experiments of low-viscosity drops oscillating in the microgravity environment of a Space Shuttle flight have shown that the frequency shift of the oscillations agrees well with the predictions of inviscid non-linear theory (Wang et al. 1996). Unprecedented microgravity observations of the maximal shape oscillations of a surfactant-bearing water drop during a mission of Space Shuttle Columbia have also been documented by Apfel et al. (1997).

In this paper, we describe two-dimensional numerical simulations of initially elongated liquid drops undergoing free oscillations in vacuum with zero gravity, using two different numerical approaches. We consider two separate sequences of calculations: one where the drops are kept isothermal with associated Reynolds numbers in the range $0.5 \leq \mathrm{Re} \leq 50$ and the other where non-isothermal conditions are adopted for $0.5 \leq \mathrm{Re} \leq 1{,}000$. We consider arbitrary viscosity and limit our analysis to non-rotating drops.

In typical experiments of shape recovery of deformed drops, the drop is first distorted in a shear flow field or by acoustic levitation. After the shear flow is abruptly stopped or the levitating force is reduced to the strength necessary to maintain the drop suspended, the transient behaviour of the extended drop proceeds in one of two ways: the drop may relax back to its original spherical shape, or, if the extension was beyond a critical aspect ratio, it may break up into a number of smaller droplets. In the present study, we will only be concerned with situations where the initial drop deformations are below the critical elongation ratio, i.e., the drop will always relax back to spheres.

## 2 Isothermally Oscillating Drops

Calculations of a fluctuating liquid drop under isothermal conditions were carried out using the JADIM code for $0.5 \leq \mathrm{Re} \leq 50$, where $\mathrm{Re} = (\rho\sigma R)^{1/2}/\eta$ is the Reynolds number, $\rho$ is the drop density, $\sigma$ is the surface tension, $R$ is the drop radius, and $\eta$ is the dynamic (shear) viscosity. We restrict ourselves to two-space dimensions so that all variables are functions of the $(x,y)$-coordinates and time $t$. In this way, the drop is represented by an infinitely thin disk, with its oscillations about the spherical shape corresponding to deformations of the disk perimeter about its unperturbed circular shape.

The JADIM code is based on a finite-volume discretization method for solving the Navier-Stokes equations, where all spatial derivatives are approximated by second-order accurate central differences, coupled to the Volume of Fluid (VOF) method for tracking and locating free surfaces and fluid-fluid interfaces (Magnaudet et al. 1995; Legendre and Magnaudet 1998; Bonometti and Magnaudet 2007). Surface tension forces are handled by adding to the Navier-Stokes equations a body force per unit volume, $\mathbf{F}_\mathrm{s} = -2\boldsymbol{\kappa}\sigma\mathbf{n}$, where $\boldsymbol{\kappa} = \nabla \cdot \mathbf{n}/2$ is the curvature of the interface and $\mathbf{n}$ is the unit normal to it. The unit vector $\mathbf{n}$ is evaluated according to $\mathbf{n} = \nabla c/[c]$, where $c$ is the colour function (or volume fraction) identifying each fluid in the system and $[c]$ is the jump in $c$ across the interface. In the VOF modulus of JADIM, the colour function is evolved by solving the transport equation

$$\frac{\partial c}{\partial t} + \mathbf{v} \cdot \nabla c = 0, \tag{1}$$

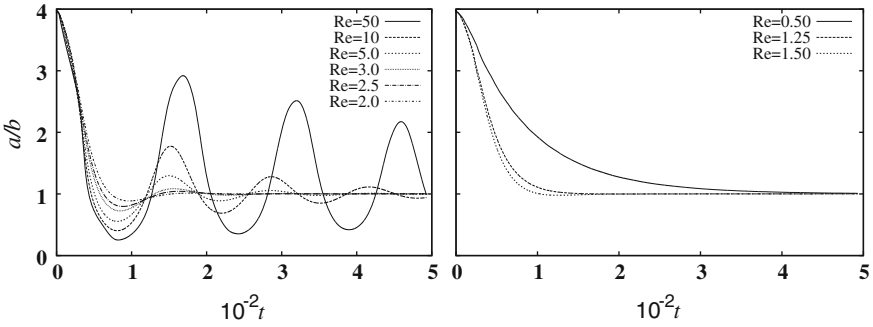


**Fig. 1** Effect of Reynolds number on the large-amplitude oscillations when a drop is released from an elliptic elongation with aspect ratio $a/b = 4$ under isothermal conditions as calculated with the JADIM code. Underdamped oscillations are shown for $2.0 \leq \mathrm{Re} \leq 50$ (*left panel*) and overdamped aperiodic returns to the circular rest state for $\mathrm{Re} \leq 1.5$ (*right panel*)

where $c = 0$ if there is no traced fluid inside the cell volume and $c = 1$ otherwise, while $0 < c < 1$ when the interphasal surface cuts the cell volume. The time integration of the equations is performed using an implicit Runge-Kutta/Crank-Nicolson algorithm so that the overall code is also second-order accurate in time. A detailed description of the JADIM code and its VOF modulus can be found in the above references, while validation of the method on the motion and deformation of fluid-fluid interfaces can be found in Legendre et al. (2003) and Merle et al. (2005).

The initial model was constructed by mapping the elliptic drop on a square grid of $64 \times 64$ elements. The drop has density $\rho \approx 1.764$, uniform temperature $T \approx 0.2$, and internal pressure $p \approx 0.156$ in reduced units. The area of the ellipse was chosen to correspond to that of a circle of radius $R \approx 12.27$. The outer vacuum was approximated by assuming an ambient fluid (continuous phase) of density and viscosity three orders of magnitude lower than the drop values. On the line borders of the square grid no-slip boundary conditions are applied. All drops start with the same parameters except for their coefficient of shear viscosity, $\eta$, which was varied to provide a set of elongated drops with $0.5 \leq \mathrm{Re} \leq 50$. Because of assumed reflection symmetry about the semi-minor and semi-major axes of the ellipse, only a quarter of the computational domain is effectively included in the calculations.

The variation of the drop aspect ratio with time is displayed in Fig. 1 for different Reynolds numbers. When Re is decreased from 50 to 2, the amplitude of the oscillations decreases as the strength of the viscous forces increases over the inertial ones. At low Reynolds ($2 \leq \mathrm{Re} \leq 5$), the drop recovers its circular shape after about three to four periods, while several more are needed for the $\mathrm{Re} \geq 10$ drops to relax back to circles. A change in the regime of the oscillations from underdamped (periodic), when $2 \leq \mathrm{Re} \leq 50$ (left panel), to critically damped, when $\mathrm{Re} = 1.5$ and 1.25 (right panel), corresponding to a fast aperiodic return to the circular shape, and then to overdamped when $\mathrm{Re} = 0.5$, corresponding to a much slower aperiodic decay mode, is clearly observed. This result is in good agreement with linear theory

which predicts an aperiodic decay mode for Re between $\approx 1.3$ and 1.768 (Prosperetti 1980). For globular drops, Basaran (1992) and Meradji et al. (2001) found the same behaviour for $1.3 < \mathrm{Re} < 1.4$ and $1.2 < \mathrm{Re} < 1.4$, respectively, when the drop is released from a second-harmonic shape with initial aspect ratio $a/b \approx 1.015$.

## 3 Non-Isothermally Oscillating Drops

The non-linear oscillations of elongated drops under non-isothermal conditions are investigated using a smoothed particle hydrodynamics (SPH) code. As before, attention is focused on large-amplitude oscillations of drops that are released from a static elliptic shape with aspect ratio $a/b = 4$ in two-space dimensions. The SPH code solves the equations of mass, momentum, and energy conservation in Lagrangian form, including the effects of viscosity and heat conduction, coupled to the vdW equations of state

$$p = \frac{\rho \bar{k}_B T}{1 - \bar{\beta}\rho} - \bar{\alpha}\rho^2, \tag{2}$$

$$U = \frac{\xi}{2}\bar{k}_B T - \bar{\alpha}\rho, \tag{3}$$

for the pressure and thermal energy, respectively. In these equations, $\xi$ is the number of degrees of freedom of the molecules ($= 2$ in two dimensions) and $\bar{k}_B = k_B/m$, where $k_B$ is the Boltzmann's constant and $m$ is the particle mass. Furthermore, $\bar{\alpha} = \alpha/m^2$ and $\bar{\beta} = \beta/m$, where $\alpha$ is the cohesive action and $\beta$ is a constant parameter due to the finite size of the particles.

The effects of surface tension are simulated here with the aid of Eq. (2) by separating the cohesive term, $-\bar{\alpha}\rho^2$, from the remainder forces in the SPH representation of the momentum equation. The same applies to the energy term, $-\bar{\alpha}\rho$, in Eq. (3). The former term contributes with an attractive central force between the SPH particles, while the latter one contributes with an effective heating due to the work done by the cohesive pressure forces on the liquid within the free surface. A predictor-corrector leapfrog scheme is used to advance the position, velocity, and thermal energy of particles in time, from which updates of the density, temperature, and pressure are computed. Numerical stability is guaranteed by limiting the time step according to the CFL condition. A detailed account of the SPH code and its applications to model free-surface phenomena can be found in López and Sigalotti (2006), Sigalotti et al. (2006) and Sigalotti and López (2008).

In contrast to the isothermal models, the elliptic elongation is now obtained by deforming a stable circular drop by means of an area-preserving coordinate transformation (Twiss and Moores 1992). A circular drop is constructed numerically by starting the calculation with a square-cell array of 900 SPH particles of equal mass, separated along the $x$ and $y$ axes by a dimensionless distance $\Delta s = 0.78$. We adopt

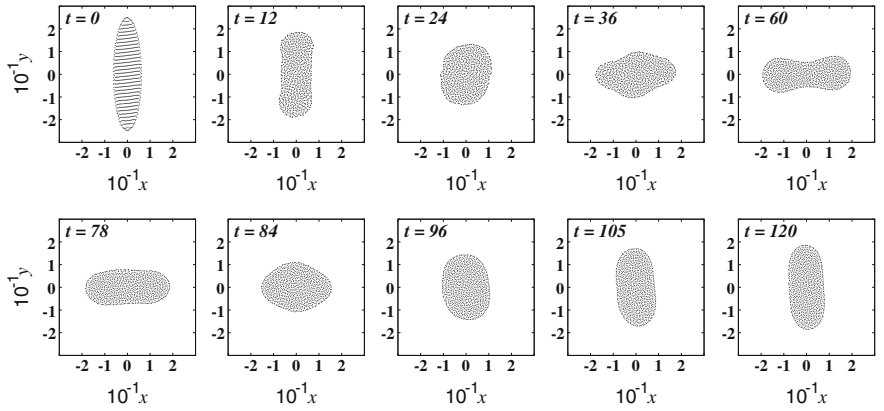


**Fig. 2** Transient shapes during the first oscillation period of a drop released from an elliptic elongation with aspect ratio $a/b = 4$ at Re $=$ 500 as calculated with the SPH code. The time is given in reduced units

$m = 1$, $\bar{\alpha} = 2$, $\bar{\beta} = 0.5$, and $\bar{k}_B = 1$ in reduced units. The initial density, $\rho_0$, and temperature, $T_0$, are chosen such that $\rho_0 < 1/\bar{\beta}$ and $\bar{k}_B T_0 > 2\bar{\alpha}\rho_0(1 - \bar{\beta}\rho_0)^2$ for thermodynamic stability. With a subcritical temperature $T_0 = 0.2$ and choosing $\eta = 1$, $\zeta = 1$, and $\kappa = 5$ in reduced units, where $\zeta$ is the bulk viscosity and $\kappa$ is the coefficient of heat conduction, a stable circular drop of central density $\rho(0) \approx 1.769$, pressure $p(0) \approx 0.162$, temperature $T(0) \approx 0.423$, radius $R \approx 12.5$, and surface tension $\sigma = p(0)R \approx 2.02$, with no external atmosphere, is formed after $t = 600$. A set of equilibrium circular drops was constructed with the same parameters as before, except that the shear viscosity was varied in the range $0.0067 \leq \eta \leq 13.36$, corresponding to Reynolds numbers in the interval $0.5 <$ Re $< 1{,}000$. Fluid motion is generated by deforming the reference circular drops into an elliptic shape via the density-conserving coordinate transformations (Twiss and Moores 1992):

$$x' = \frac{x}{1+\varepsilon}, \qquad y' = (1+\varepsilon)y, \tag{4}$$

where $\varepsilon$ is the elongation given by $\varepsilon = (a/b)^{1/2} - 1$. An ellipse with aspect ratio $a/b = 4$ is obtained by setting $\varepsilon = 1$ in Eq. (4).

The time resolved evolution of a drop for Re $= 500$ is displayed in Fig. 2 during its first period of oscillation. The drop first contracts along its major axis as part of its surface energy is transformed into internal liquid movement, passing through a transient approximate circular shape ($t = 24$) before reaching a maximum elongation along the $x$-axis ($t = 60$). At this point, the rim pressure exceeds the stagnation pressure inside the drop, causing it to contract back under surface tension and reach a prolate shape after completion of the first oscillation period ($t = 120$). The variation of the drop aspect ratio with time is shown in Fig. 3 for all runs. At comparable Re the drops oscillate with lower amplitudes and undergo stronger dissipation than the

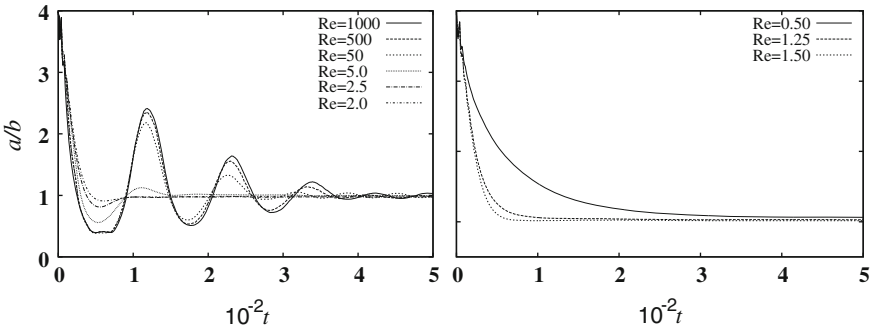


**Fig. 3** Effect of Reynolds number on the large-amplitude oscillations when a drop is released from an elliptic elongation with aspect ratio $a/b = 4$ under non-isothermal conditions as calculated with the SPH code. Underdamped oscillations are shown for $2.0 \leq \mathrm{Re} \leq 1{,}000$ (*left panel*) and overdamped aperiodic returns to the circular rest state are obtained for $\mathrm{Re} \leq 1.5$ (*right panel*)

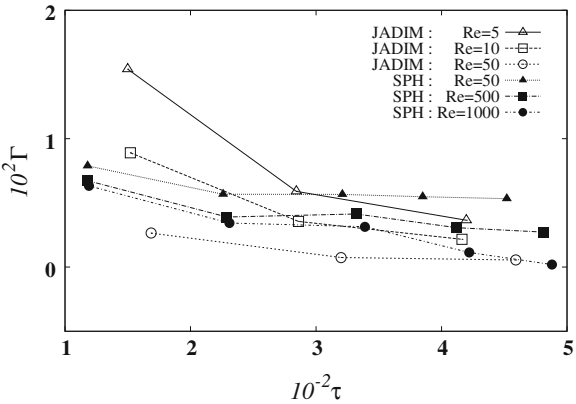


**Fig. 4** Variation of the decay factor over several periods of oscillation for all runs: JADIM simulations (*open symbols*) and SPH calculations (*filled symbols*)

isothermal models of Fig. 1. The damping of the oscillations is mostly due to viscous dissipation and, to some extent, to the finite heat conductivity. The transition from periodic to aperiodic decay occurs at the same Re predicted by the isothermal models, suggesting that it is independent of the initial drop parameters and mechanisms of dissipation.

Finally, Fig. 4 shows how the decay factor (or damping rate), defined as

$$\Gamma_n = \frac{1}{\tau_n} \ln \left[ \frac{(a/b-1)_{\tau_{n-1}}}{(a/b-1)_{\tau_n}} \right] \qquad n = 1, 2, ..., \tag{5}$$

varies as a function of the oscillation period for both the isothermal and non-isothermal models, where $n$ is the period number. For all Reynolds numbers, the

damping rate decreases with increasing period number, decaying most rapidly during the first period and changing only slightly with increasing time. Evidently, the lower is the Reynolds number, the higher is the damping rate.

## 4 Conclusions

We have presented two-dimensional calculations of the free oscillations of a viscous elongated drop surrounded by a vacuum in microgravity. The full Navier-Stokes equations with appropriate interfacial treatment were solved, using a finite-volume code under isothermal conditions and an SPH-based code under non-isothermal conditions, including the effects of heat conduction.

The main characteristics of drop relaxation back to its stable circular shape, with transition from periodic to aperiodic decay of the oscillations as viscosity is increased, are found in good agreement with linear theory and previous simulations. We find that heat conduction is an important additional mechanism for enhancing dissipation at moderate to high Reynolds numbers.

## References

Apfel RE, Tian Y, Jankovsky J, Shi T, Chen X, Holt RG, Trinh E, Croonquist A, Thornton KC, Sacco A Jr, Coleman C, Leslie FW (1997) Free oscillations and surfactant studies of superdeformed drops in microgravity. Phys Rev Lett 78:1912–1915

Basaran OA (1992) Nonlinear oscillations of viscous liquid drops. J Fluid Mech 241:169–198

Becker E, Hiller WJ, Kowalewski TA (1991) Experimental and theoretical investigation of large-amplitude oscillations of liquid droplets. J Fluid Mech 231:189–210

Becker E, Hiller WJ, Kowalewski TA (1994) Nonlinear dynamics of viscous droplets. J Fluid Mech 258:191–216

Bonometti T, Magnaudet J (2007) An interface-capturing method for incompressible two-phase flow: validation and application to bubble dynamics. Int J Multiph Flow 33:109–133

Legendre D, Magnaudet J (1998) The lift force on a spherical bubble in a viscous linear shear flow. J Fluid Mech 368:81–126

Legendre D, Magnaudet J, Mougin G (2003) Hydrodynamic interactions between two spherical bubbles rising side by side in a viscous liquid. J Fluid Mech 497:133–166

López H, Sigalotti L Di G, (2006) Oscillations of viscous drops with smoothed particle hydrodynamics. Phys Rev E 73:051201

Lundgren TS, Mansour NN (1988) Oscillations of drops in zero gravity with weak viscous effects. J Fluid Mech 194:479–510

Magnaudet J, Rivero M, Fabre J (1995) Accelerated flows around a rigid sphere or a spherical bubble. Part I: steady straining flow. J Fluid Mech 284:97–135

Mashayek F, Ashgriz N (1998) Nonlinear oscillations of drops with internal circulation. Phys Fluids 10:1071–1082

Meradji S, Lyubimova TP, Lyubimov DV, Roux B (2001) Numerical simulation of a liquid drop freely oscillating. Cryst Res Technol 36:729–744

Merle A, Legendre D, Magnaudet J (2005) Forces on a high-Reynolds-number spherical bubble in a turbulent flow. J Fluid Mech 532:53–62

Miller AC, Scriven LE (1968) The oscillation of a fluid droplet immersed in another fluid. J Fluid Mech 32:417–435
Moran K, Yeung A, Masliyah J (2003) Shape relaxation of an elongated viscous drop. J Colloid Interface Sci 267:483–493
Prosperetti A (1980) Free oscillations of drops and bubbles: the initial-value problem. J Fluid Mech 100:333–347
Rayleigh JWS (1879) On the capillary phenomena of jets. Proc R Soc Lond 29:71–97
Reid WH (1960) The oscillations of a viscous liquid drop. Q Appl Math 18:86–89
Sigalotti L Di G, Daza J, Donoso A (2006) Modelling free surface flows with smoothed particle hydrodynamics. Condens Matter Phys 9:359–366
Sigalotti L Di G, López H (2008) Adaptive kernel estimation and SPH tensile instability. Comput Math Appl 55:23–50
Trinh E, Wang TG (1982) Large-amplitude free and driven drop-shape oscillations: experimental observations. J Fluid Mech 122:315–338
Tsamopoulos JA, Brown RA (1983) Nonlinear oscillations of inviscid drops and bubbles. Int J Fluid Mech 127:519–537
Twiss RJ, Moores EM (1992) Structural geology. Freeman, New York
Wang TG, Anilkumar AV, Lee CP (1996) Oscillations of liquid drops: results from USML-1 experiments in space. J Fluid Mech 308:1–14